Autonomous division of the outer membranes in Gram-negative bacteria

Carolina Basurto De Santiago, Carlos A. Ramírez Carbó and Beiyan Nan*

Department of Biology, Texas A&M University, College Station, Texas, USA

*Correspondence: Beiyan Nan, bnan@tamu.edu

Abstract

Gram-negative bacteria divide by separating two cell wall layers: peptidoglycan (PG) and the outer membrane (OM). In certain model organisms, the OMs are tethered to PG, ensuring it closely follows PG when cells constrict at division sites. In contrast, the OMs of *Myxococcus xanthus* exhibit slight invagination at the onset of cell division but do not follow the constriction of PG, instead separating significantly later, only after complete PG fission. However, reinforcing the OM-PG connection by overexpressing tethering proteins, either the endogenous Pal or the exogenous Lpp, synchronizes the constriction of both layers. Our findings suggest that OMs can divide by simple mechanical force. The variability in OM division mechanisms among Gram-negative bacteria reflects differences in both the mode of PG division and the strength of PG-OM interactions.

Introduction

The cell wall of Gram-negative bacteria consists of two distinct layers: a peptidoglycan (PG) meshwork and an outer membrane (OM). PG is a single macromolecule of glycan strands crosslinked by short peptides. The OM is an asymmetric bilayer with lipopolysaccharides (LPS) in the outer leaflet and phospholipids in the inner leaflet[1]. While PG plays a major role in maintaining cell integrity and morphology, the OM serves as a selective barrier that protects the cell from harmful substances, including antibiotics[2,3]. In certain bacteria, such as *Escherichia coli*, OMs are load-bearing structures that can exhibit even greater stiffness than PG[4,5]. During cell division, Gram-negative bacteria must separate both the PG and OM layers. This process can be conceptually divided into three stages: (i) constriction, where PG is assembled inward at division site, leading to localized narrowing of cell body; (ii) cytokinesis, marked by cytoplasmic and inner membrane (IM) division following PG fission; and (iii) OM fission (**Fig. 1**).

Cells divide their PG using a well-organized PG remodeling machinery called the divisome[6] although the mechanisms driving constriction can differ. For example, *E. coli* separates daughter cells by forming a septum PG perpendicular to the cell's long axis[7-9], whereas *Caulobacter crescentus* "pinches" PG inward at the division site without producing a septum[10] (**Fig. 1**). In contrast, the mechanisms underlying OM division remain less understood, as the OMs of Gram-negative bacteria are devoid of energy sources and therefore lack dedicated division machinery.

Many Gram-negative bacteria tether their OMs to PG. For instance, *E. coli* employs multiple systems to tether the OM to PG (**Fig. 1**). First, the PG-associated lipoprotein (Pal) that attaches to PG noncovalently and connects to the OM components in the Tol-Pal system, accumulates at the division site[11,12]. Second, the OM contains abundant Braun's lipoprotein (Lpp) that attaches to PG directly through covalent bonds[13]. Although Lpp is absent from the constriction site during division, it can functionally compensate for the

43 loss of Pal because the simultaneous absence of both Pal and Lpp disrupts coordination
44 between the PG layer and the OM during division[14]. Third, the OM lipoprotein LpoA and
45 LpoB directly interact with PG synthases to coordinate the growth and division of these
46 two cell wall layers[15-18]. Fourth, some β-barrel OM proteins (OMPs) interact with PG
47 noncovalently through their C-terminal OmpA-like domains[19]. Through these tethering
48 mechanisms, the *E. coli* OM closely follows PG during constriction, forming a deep V-
49 shaped invagination[7,16] (**Fig. 1**). As the divisome assembles the septum toward the center
50 of cell, the distance between the OM and PG remains remarkably consistent (**Fig. 1**)[8,9],
51 reflecting their tight coordination during cell division. *C. crescentus* does not produce Lpp
52 or LpoA/B but does encodes Pal and OmpA-like proteins. During the gradual constriction
53 of *C. crescentus*, its OM also remains attached to the PG layer until just before cytokinesis.
54 At that stage, the PG separates first, leaving the two daughter cells connected by a narrow
55 OM bridge, sometimes as small as 60 nm in diameter[10] (**Fig. 1**).
56

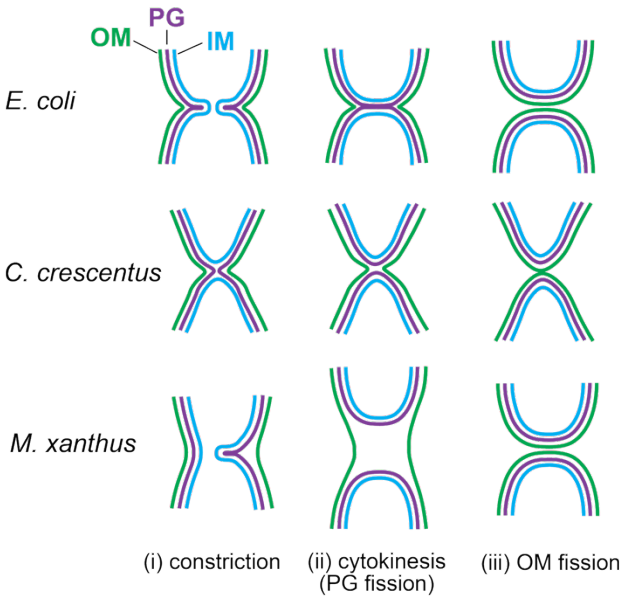

57

58 **Fig. 1. Variation in division mechanisms among Gram-negative bacteria.** Despite that *E. coli*
59 forms septum but *C. crescentus* does not, the OMs of both bacteria closely follow PG during
60 constriction. In contrast, *M. xanthus* OM does not follow PG during restriction and eventually
61 separates significantly later after cytokinesis.
62

63 In both *E. coli* and *C. crescentus*, how OMs separate after cytokinesis is less
64 understood. It is unclear if the coordinated constriction of PG and OM is a universal
65 division mechanism among Gram-negative bacteria and if the connection between OM
66 and divisome is essential for OM division. To answer these questions, we investigated
67 cell division in *Myxococcus xanthus*, a rod-shaped Gram-negative bacterium[20]. In contrast
68 to the rigid *E. coli* OM, the *M. xanthus* OM appears highly fluid, enabling the rapid
69 diffusion of OM proteins, frequent shedding of OM, and active intercellular exchange of
70 OM contents among closely related strains[21-23]. Thus, *M. xanthus* may exemplify a wide
71 group of Gram-negative bacteria that lack rigid connections between the OM and PG.
72 Using bright field microscopy, *in situ* cryogenic electron microscopy (cryoEM), and
73 fluorescence microscopy, we found a significant disconnection between the PG and OM
74 during *M. xanthus* division. Its OMs do not follow the constriction of PG, instead
75 separating significantly later, after cytokinesis. However, reinforcing the OM-PG
76 connection by overexpressing the endogenous tethering protein Pal synchronizes the
77 constriction of both layers. We propose that OMs may separate by mechanical forces and
78 that the diversity in OM dynamics during cell division reflects a spectrum, with each
79 organism's position determined by the strength of its PG-OM interactions.

Results

M. xanthus daughter cells remain transiently connected through their OMs after cytokinesis

M. xanthus lacks flagella and cannot swim. Instead, it moves across surfaces using two distinct mechanisms: a twitching-like motility driven by type IV pili (T4P) and a gliding motility powered by fluid motor complexes[24,25]. During imaging of *pilA*⁻ cells, which lack T4P and rely solely on gliding for movement, we frequently observed cell division. Under a differential interference contrast (DIC) microscope, cytokinesis in *M. xanthus* cells generated regions of reduced cell mass at division sites, which appeared as pale zones (**Fig. 2A**) reminiscent of the enlarged periplasmic spaces in plasmolyzed *E. coli* cells, where the IMs separate from the OMs[4,26,27]. Distinctly different from *E. coli* and *C. crescentus* that display significant cell envelope constriction at division sites[9,10] (**Fig. 2B**), dividing *M. xanthus* cells only narrowed slightly between nascent daughter cells even after cytokinesis (**Fig. 2A**).

Due to the asymmetric distribution of polarity regulators in mother cells, daughter cells are programmed to move in opposite directions after division[28]. Using time-lapse microscopy, we visualized the separation of nascent daughter cells and observed a remarkable "tug-of-war" behavior. To minimize interference from neighboring cells, we restricted our analysis to division events where the cells remained isolated throughout the entire process. Across all 37 analyzed division events, the daughter cells exhibited semi-random, short-range movements (< 5 μm) before fully separating. They alternated between moving together in one direction and then the opposite, and occasionally approached each other, causing buckling at the division site. Throughout this process, the daughter cells remained connected, with the intercellular space fluctuating—either stretching to ~ 1 μm or compressing to 0 μm (**Fig. 2A, Movie S1**).

As the *pilA*⁻ cells lack both T4P and extracellular polysaccharides, the major

106 structures *M. xanthus* utilize to connect individual cells[29,30], we hypothesize that nascent
107 daughter cells connect to each other transiently through OMs. To test this hypothesis, we
108 proceeded to image cytokinesis and OM fission using fluorescence microscopy. Wheat
109 germ agglutinin (WGA) was reported to specifically bind to the OMs of *E. coli*[31]. To access
110 WGA binding specificity in *M. xanthus* cells, we stained the entire OMs of cells expressing
111 mCherry-labeled AglR, an IM protein part of a proton channel[32], with Alexa Fluor 488-
112 conjugated WGA for 1 h, then transferred cells to water. After this hypoosmotic shock,
113 cells were plasmolyzed, i.e. the IMs shrank and separated from OMs[5,33]. While the IMs
114 retained their original shape, the OMs frequently formed large bulges, which were
115 specifically stained by WGA (**Fig. 2C**). Thus, WGA specifically labels the OMs in *M.*
116 *xanthus*.
117

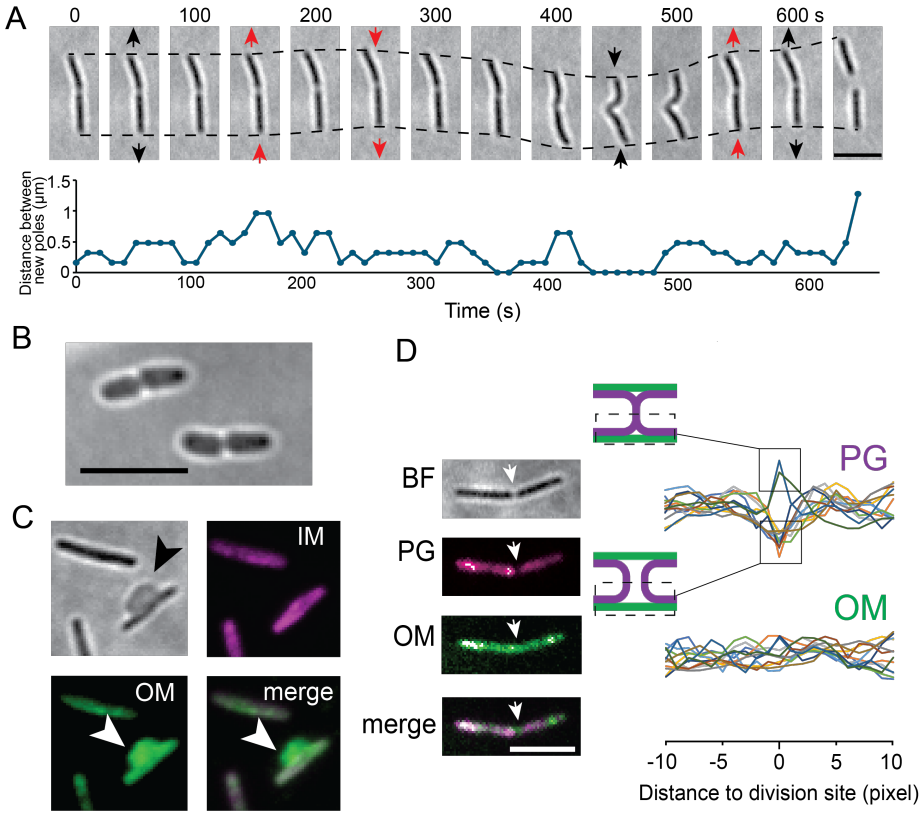

118

119 **Fig.2. *M. xanthus* OMs sperate later than cytokinesis. A)** Nascent daughter cells move in a
120 tug-of-war manner on an agar surface (also see **Movie S1**). Black arrows indicate frames where

121 the daughter cells move in opposite directions, while red arrows indicate frames where they move
122 together in the same direction. The positions of old cell poles are marked by dotted lines and the
123 distance between the new cell poles is displayed frame by frame. **B)** Dividing *E. coli* MG1655
124 cells that typically display deep constrictions at division sites. **C)** Plasmolysis assay indicates that
125 WGA specifically label the OMs of *M. xanthus*. The IMs are labeled by AglR-GFP. White arrows
126 point to an OM bulge formed under hypoosmotic shock, which was specifically stained by Alexa
127 Fluor 488-conjugated WGA. **D)** Whereas the fluorescence signals of TADA-labeled PG either
128 peak or plunge at the division sites, corresponding to septum assembly and cytokinesis,
129 respectively, the WGA-labeled OMs remain connected. Images of a typical pair of daughter cells
130 are shown on the left where white arrows point to the division sites. The fluorescence intensities
131 of PG and OMs from 12 cells are shown on the right. The sections of cells imaged using our setup
132 are marked by boxes of dashed lines and the identities of cells are distinguished by colors, and
133 the fluorescence intensity values were normalized using Z-score standardization. Scale bars, 5
134 μm.
135

136 To visualize PG and OMs simultaneously during division, we grew *pilA*$^{-}$ cells
137 overnight in the presence of TAMRA 3-amino-D-alanine (TADA) before WGA staining.
138 TADA is a red fluorescent D-amino acid that is incorporated into PG by PG synthases[34].
139 We selected dividing cells with cytoplasms separated by fewer than 3 pixels (480 nm) in
140 DIC images and used fluorescence microscopy to visualize a ~200-nm-thick longitudinal
141 section encompassing both the PG and OMs. Imaging was performed under highly
142 inclined and laminated optical sheet (HILO) illumination[32,35-37], which enabled near even
143 illumination of the cell surfaces facing the coverslip. Fluorescence signals of PG at
144 division sites reflected the progression of cytokinesis: intensified signals indicated septal
145 PG growth, whereas loss of fluorescence signified complete PG fission (**Fig. 2D**).
146 Regardless of the status of PG, all the dividing cells (n > 100) displayed continuous OM
147 at their division sites (**Fig. 2D**). Crucially, we never detected a surge in OM signal at
148 division sites, suggesting that, unlike PG, *M. xanthus* OMs do not undergo gradual
149 invagination (**Fig. 2D**). These distinct staining patterns also indicate that WGA did not
150 stain PG. Taken together, these observations confirmed our hypothesis that after
151 cytokinesis, nascent daughter cells are still transiently connected by OMs.

152 **Significant OM invagination does not occur in *M. xanthus* during cell division**

153 To investigate OM fission at high resolution, we captured the micrographs of
154 dividing *M. xanthus* cells using cryoEM, in which the electron densities of the IMs and
155 OMs were easily distinguished from the background (**Fig. 3A**). In contrast, the thin PG
156 layer was extremely difficult to visualize (**Fig. 3A**). In this case, we use IMs, instead of the
157 PG, to monitor cytokinesis. Due to the long generation time of *M. xanthus* (~4 h)[28], locating
158 individual dividing cells on EM grids was extremely difficult. After screening more than
159 1,000 cells, we identified 17 at the constriction stage (**Fig. 3A, 3B**) and 10 pairs of daughter
160 cells that had completed cytokinesis (**Fig. 3C–E**). Among the 17 constricting cells, the IMs
161 exhibited varying degrees of invagination, whereas the OMs only constricted slightly,
162 regardless of the extent of IM invagination (**Fig. 3A, 3B**). Consequently, we did not
163 observe any deep V-shaped OM invaginations, a feature commonly seen in dividing *E.*
164 *coli* cells[7]. Unexpectedly, we found that the IMs of all the 17 constricting cells invaginated
165 in an asymmetric pattern, suggesting asymmetric septum growth (**Fig. 3A, 3B**). Both the
166 loss of synchronized constriction between OMs and IMs and the asymmetric invagination
167 of IMs are strikingly similar to two *E. coli* filamentous mutants that cannot separate
168 daughter cells: the *ΔenvC ΔnlpD* mutant that cannot hydrolyze septal PG[7] and the *Δlpp*
169 *Δpal* strain that loses the major connections between PG and OM[14]. However, *pilA*$^-$ *M.*
170 *xanthus* cells do not form cell chains, indicating that the uncoupled invagination of OMs
171 and IMs does not lead to division defects.

172 To further investigate the asymmetry of cell constriction, we constructed a
173 merodiploid *ftsZ*$^+$/*ftsZ-gfp* strain that expressed green fluorescent protein (GFP)-labeled
174 FtsZ using its native promoter at the Mx8 phage attachment site[38]. FtsZ-GFP formed
175 bright clusters near the longitudinal center of many cells, marking the assembly of the
176 cytokinetic Z-ring (**Fig. 3G**). Among the 105 cells with FtsZ clusters, 97 (92.3%) positioned
177 these clusters asymmetrically, offset from their long cell axes (**Fig. 3G, 3H**), consistent
178 with cryoEM observations.

179 Among the 10 daughter cell pairs that had completed cytokinesis, 9 remained
180 connected by the OMs of the mother cells (**Fig. 3C - E**). Between these nascent daughter
181 cells, the distance between IMs at the new cell poles ranged from approximately 20 nm
182 (**Fig. 3C, 3D**) to about 500 nm (**Fig. 3E**). Consequently, their OMs were either relaxed (**Fig.**
183 **3C**), folded on one side and stretched on the other (**Fig. 3D**), or stretched and even twisted
184 (**Fig. 3E**). Interestingly, OM bulges, the common indicators of the detachment between
185 OM and PG[5], were observed at sites where OMs were stretched (**Fig. 3E**).
186 The stretched OMs at the division sites confirms our findings from DIC (**Fig. 2A,**
187 **Movie S1**) and single-particle microscopy[21] imaging that *M. xanthus* OMs are elastic and
188 fluid. This elasticity suggests that OMs might separate through a mechanical stretch-and-
189 snap mechanism after cytokinesis. However, fluorescence microscopy at up to 67 Hz (15
190 ms/frame) failed to capture such snapping events, suggesting they occurred faster than
191 our detection threshold. Nevertheless, cryoEM imaging revealed one instance of
192 stretched and ruptured OMs between separating daughter cells (**Fig. 3F**).
193

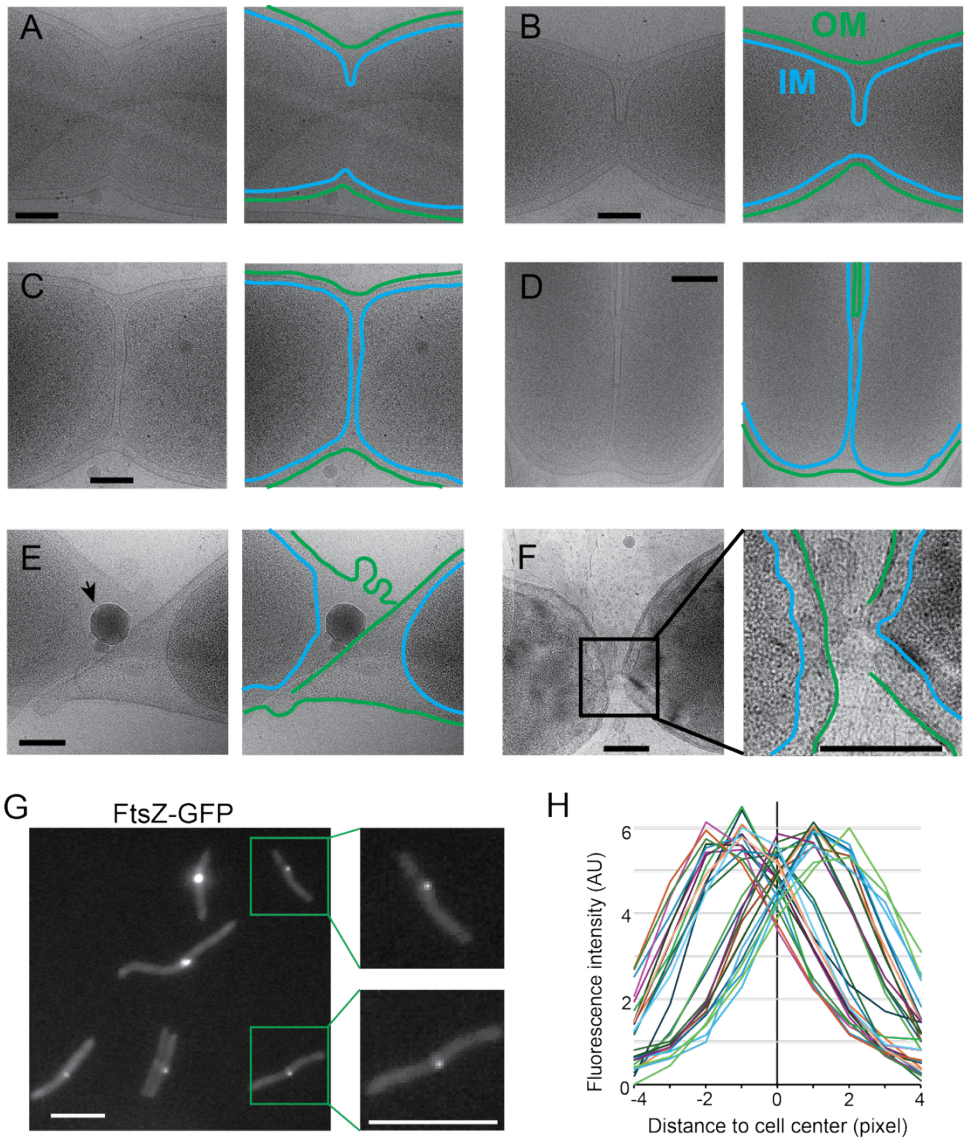

Fig. 3. Significant OM invagination does not occur in *M. xanthus* during cell division. CryoEM images of cells at the stage s of constriction (**A, B**), cytokinesis (**C – E**), and OM fission (**F**). When the OM stretched significantly between daughter cells, OM bulges also emerged (**E**). **G**) FtsZ-GFP localizes in an asymmetric manner in dividing *M. xanthus* cells. **H**) The fluorescence intensities of FtsZ-GFP from 27 cells across cell width. The centers of cells are designated as 0 and the identities of cells are distinguished by colors, and the fluorescence intensity values were normalized using Z-score standardization. The arrow in panel E points to an ice particle. Scale bars, A – F, 200 nm; G, 5μm.

Enhanced OM-PG connection synchronizes the constriction of both layers

Similar to most Gram-negative bacteria, *M. xanthus* possesses a conserved Tol-Pal system and several OmpA-like OMPs[39], albeit cryoEM and fluorescence imaging

207 demonstrated that their native expression fails to couple the OM to PG during division
208 (**Fig. 2, 3**). To examine how PG-tethering influences the mode of OM division, we
209 overexpressed the native Pal as a merodiploid in *M. xanthus* using a vanillate-inducible
210 promoter[40]. Under conditions of excess Pal, OM fluorescence rose and fell in synchrony
211 with PG fluorescence (**Fig. 4A**), suggesting tight coupling between these two layers
212 during constriction and cytokinesis. Consistently, cryoEM analysis revealed that OM
213 constrictions tracked IMs closely in all 7 dividing cells observed (**Fig. 4D**), a pattern not
214 observed in the parental *pilA*$^{-}$ cells. Although *M. xanthus* lacks Lpp-like proteins, it
215 encodes two putative L,D-transpeptidases, the enzymes that catalyze the covalent
216 linkage between the terminal lysine residue of Lpp and the stem peptides of PG in *E. coli*[41].
217 To test if introducing *E. coli* Lpp into *M. xanthus* could strengthen the OM-PG connection
218 and thus synchronize their constriction during cell division, we used the same vanillate-
219 inducible promoter to express wild-type *E. coli* Lpp exogenously. Remarkably, like Pal,
220 overexpressed Lpp synchronized OM and PG constriction in fluorescence images (**Fig.**
221 **4B**) and OM and IM constriction in all 12 cryoEM micrographs (**Fig. 4E**). These
222 observations suggest that *M. xanthus* can crosslink Lpp to PG, enabling OMs to constrict
223 in concert with PG and IMs at division sites. To confirm this observation, we
224 overexpressed an Lpp variant that lacks the terminal lysine residue (Lpp$_{\Delta K}$) and therefore
225 is unable to form covalent bonds with PG[41]. Overexpressed Lpp$_{\Delta K}$ failed to synchronize
226 OMs with either PG (**Fig. 4C**) or IMs (**Fig. 4F**). Thus, reinforcing the OM-PG connection,
227 either by endogenous or exogenous coupling proteins, is sufficient to synchronize their
228 constriction during cell division. In stark contrast to their parental strain (**Fig. 3A, 3B**),
229 cells overexpressing Pal and Lpp displayed symmetric IM invaginations, suggesting that
230 the degree of OM-PG connection also regulates septum growth.

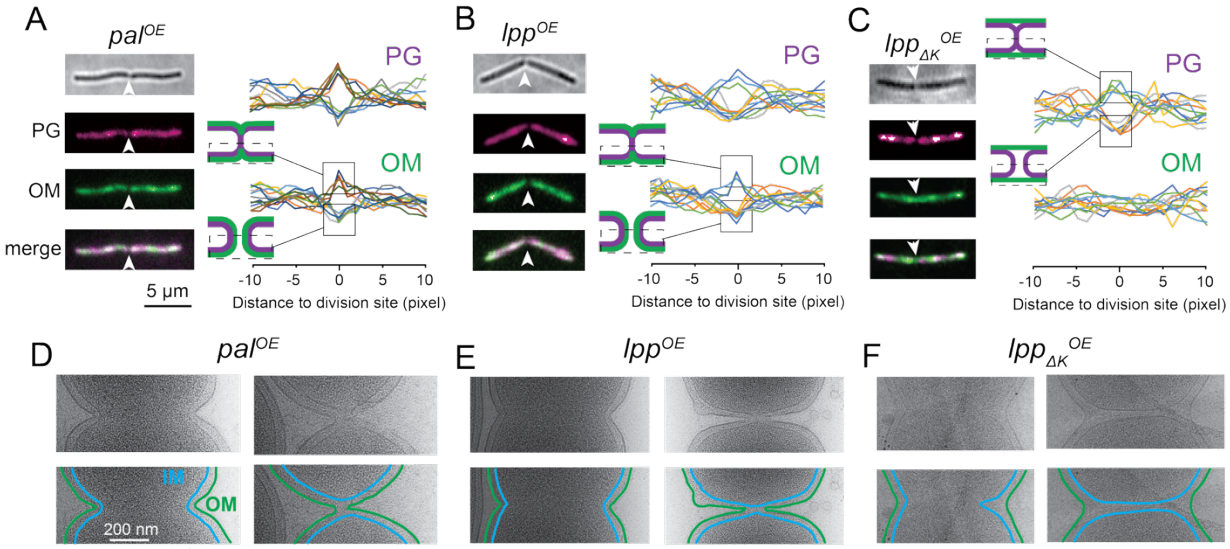

Fig. 4. Enhanced OM-PG connection synchronizes the constriction of both layers. A - C) Fluorescence images of typical dividing cells that overexpress native Pal (**A**), wild-type *E. coli* Lpp (**B**) and an *E. coli* Lpp variant that lacks the lysine residue that attaches OM to PG ($Lpp_{\Delta K}$, **C**). The PG and OMs of cells are labeled with TADA and Alexa Fluor 488-conjugated WGA, respectively. White arrows point to the division sites. The fluorescence intensities of PG and OMs from 12 cells are shown on the right. The sections of cells imaged using our setup are marked by boxes of dashed lines and the identities of cells are distinguished by colors, and the fluorescence intensity values were normalized using Z-score standardization. **D – F)** representative cryoEM images of the division sites in cells at the constriction (left) and cytokinesis (right) stages.

241 **Discussion**

242 OMs and PG are essential components of Gram-negative bacteria. PG forms a rigid cage
243 that protects against cell lysis, while OMs act as permeability barriers that restrict the
244 entry of hydrophobic molecules[42] and serve as load-bearing structures that maintain cell
245 morphology together with PG[4,5]. Whereas PG synthesis has long been a primary target
246 for antibiotic development, OMs are increasingly recognized as promising targets for
247 antibacterial therapies and as platforms for vaccine development[1]. Recent studies reveal
248 that OMs and PG function as an integrated cell envelope rather than independent layers.
249 Their physical linkage makes the periplasm a mechanical unit that balances turgor across
250 the inner membrane[5]. In *E. coli*, the thickness of the periplasm, determines by Lpp, is also
251 critical for signaling across the cell envelope[43]. Furthermore, PG synthesis stimulates OM
252 biogenesis in *Pseudomonas aeruginosa*[44] and PG maturation controls OM protein assembly
253 in *E. coli*[15]. It is reasonable to assume that, to preserve cell integrity these two rigid layers
254 must constrict and divide in a coordinated manner during cell division. Indeed, such
255 coordination has been documented in *E. coli*[16-18] and *C. crescentus*[10], although the
256 underlying mechanisms may vary by species. However, whether PG tethering is essential
257 for OM fission remains unresolved.

258 Our findings demonstrate that coupled constriction PG and OMs is not a universally
259 conserved mechanism for cell division. Despite lacking a tight OM-PG connection, *M.*
260 *xanthus* divides its OMs normally, although OM constriction does not occur in synchrony
261 with the PG and IMs. Live-cell and cryoEM imaging reveal that *M. xanthus* OMs are
262 highly elastic, and we propose that this elasticity may represent a conserved trait among
263 Gram-negative bacteria. For instance, while *E. coli* OMs can be even stiffer than the PG
264 layer[4], their elasticity becomes evident under hypoosmotic shock, where they form large
265 bulges without rupturing[5]. In contrast, the IMs appear far less elastic, where even a
266 moderate expansion can lead to cell lysis[5].

267 Another open question in Gram-negative bacteria cell division is how OMs complete
268 division following cytokinesis. For example, during *E. coli* division, the OMs invaginate
269 in concert with the PG through most of the constriction phase[7]. But what mechanism
270 drives OM fission once the septal PG has split? Similarly, *C. crescentus* OMs continue to
271 follow PG invagination even deeper, leaving daughter cells connected only by OM tubes
272 about 60 nm wide[10]. What force ultimately severs these OM tubes? The absence of OM
273 constrictions in dividing *M. xanthus* cells presents an extreme case, suggesting that OM
274 fission may occur autonomously through a purely physical process, independent of PG-
275 tethering. Detached from PG and lacking a dedicated division apparatus, OMs might
276 separate solely through stretching forces that surpass their elastic limit, potentially driven
277 by Brownian motion in liquid, cell motility, or growth. Ruptured OMs may
278 spontaneously reseal and reestablish their connection with the PG through their inherent
279 elasticity. Capturing such rapid OM fission events requires live-cell imaging with high
280 speed and sensitivity.

281 Our third key finding is that bacteria can tolerate a broad range of OM-PG tethering
282 strengths. For instance, although Lpp or Pal are important for OM stability in *E. coli* and
283 their absence often causes OM to blebbing, neither protein is essential for cell division[45,46].
284 Conversely, reinforcing the OM-PG connection does not impede *M. xanthus* division.
285 These observations suggest that OMs may have evolved later than PG during evolution
286 and that both OMs and their connections to PG are less conserved than the PG structure
287 itself.

288 **Materials and methods**

289 Vegetative *M. xanthus* cells were grown in liquid CYE medium (10 mM MOPS pH 7.6,
290 1% (w/v) Bacto™ casitone (BD Biosciences), 0.5% yeast extract and 8 mM $MgSO_4$) at
291 32 °C, in 125-ml flasks with vigorous shaking, or on CYE plates that contains 1.5% agar.
292 We used strain DZ2 as the wild-type *M. xanthus* strain[47]. Overexpression mutants were
293 constructed by electroporating DZ2 cells with 4 μg of plasmid DNA. The genes, driven
294 by a vanillate-inducible promoter, were inserted into the Mx4 phage attachment site as
295 merodiploid on the *M. xanthus* chromosome. Transformed cells were plated on CYE
296 plates supplemented with 10 mg/ml tetracycline and expression was induced by 100
297 μM sodium vanillate. The strains and plasmids used in this study are listed in **Table S1**.

298 **Table S1. Strains and plasmids used in this study**

Strain	Description	Source
DZ2	The wild-type strain	47
DZ4469	DZ2 *pilA::tet*	48
BN380	DZ4469 P_{van}-*lpp*	This study
BN381	DZ4469 P_{van}-$lpp_{\Delta K}$	This study
BN382	DZ4469 P_{van}-*pal*	This study
BN383	DZ2 *ftsZ-gfp*	This study
Plasmid		
pMR3629	Plasmid carrying a vanilate-induced promoter, tet^R	40
pMR3629-*lpp*	P_{van}-*lpp* in pMR3629, tet^R	This study
pMR3629-$lpp_{\Delta K}$	P_{van}-$lpp_{\Delta K}$ in pMR3629, tet^R	This study
pMR3629-*pal*	P_{van}-*pal* in pMR3629, tet^R	This study
pKA51	P_{ftsZ}-*ftsZ-gfp, Mx8 attB*, tet^R	38

299 Bacterial strains were grown overnight in CYE media with appropriate antibiotics,
300 incubated with shaking at 32 °C and 250 rpm to an optical density of OD_{600} 0.6. Cells were
301 collected by centrifugation (3 min, 6,000 × g, 25 °C) and resuspended in CYE media to a
302 final OD_{600} 12. This cell suspension (3 μl) was applied to C Flat-1.2/1.3 200 mesh copper
303 grids (Electron Microscopy Sciences) that were glow discharged for 30 seconds at 15 mA.
304 Grids were plunge-frozen in liquid ethane with an FEI Vitrobot Mark IV (Thermo Fisher
305 Scientific) at 4 °C, 100% humidity with a waiting time of 30 s, two-side blotting time of

306 2.5 - 3 s, and blotting force of 0. All subsequent grid handling and transfers were
307 performed in liquid nitrogen. Grids were clipped onto cryo-FIB autogrids (Thermo Fisher
308 Scientific).

309 Images were acquired using a Thermo Fisher Scientific Titan Krios G4 transmission
310 electron microscope, equipped with a Gatan K3 direct electron detector and a Gatan
311 BioContinuum energy filter. Imaging was performed using a 15 eV slit width on the
312 energy filter to enhance image contrast. Micrographs were recorded in counted mode at
313 a nominal magnification of 33,000x, using a dose rate of 14.65 electrons/pixel/second over
314 a 2.6-second exposure, resulting in a total accumulated dose of 50 electrons/$Å^2$.

315 For fluorescence microscopy, cultures were grown in liquid CYE overnight in the
316 presence of 75 μM TADA to OD_{600} ~1, supplemented with 10 μg/mL Alexa Fluor-488
317 conjugate WGA, and grown for one hour. Cells were spun down at 6,000 x g for 3 min
318 and the pellet washed three times with CYE. 5 μl of cells were spotted on agar (1.5%)
319 pads and imaged using a Andor iXon Ultra 897 EMCCD camera (effective pixel size 160
320 nm) on an inverted Nikon Eclipse-Ti™ microscope with a 100 × 1.49 NA TIRF objective.
321 Fluorescence of TADA and Alexa Fluor 488-conjugated WGA was excited by the 561-nm
322 and 488-nm lasers, respectively. Fluorescence intensities were quantified using the
323 ImageJ suite (https://imagej.net) and normalized by Z-score standardization using $Z = (\chi$
324 $- \mu)/\sigma$, where Z, χ, μ, and σ are the standard score, observed value, mean, and standard
325 deviation, respectively.
326

327 **Movie S1.** Time-lapse video of a dividing cell moving on a 1.5% agar surface. Images
328 were captured at 10-s intervals and played at 10 frames/s (100 x speedup).

Acknowledgments

We thank Drs. Michael Van Nieuwenhze and Yen-Pang Hsu for providing TADA, Drs. Anke Treuner-Lange and Lotte Sogaard-Andersen for the pKA51 plasmid, and Dr. Gaya Yadav for the assistance on cryoEM imaging. Part of this work was supported by the National Institutes of Health grants GM129000 to B. N.. We received financial support from Dr. David R. Zusman, who played no role in the design, execution, or presentation of this work.

References

1 Henderson, J. C. *et al.* The Power of Asymmetry: Architecture and Assembly of the Gram-Negative Outer Membrane Lipid Bilayer. *Annu Rev Microbiol* **70**, 255-278 (2016). https://doi.org/10.1146/annurev-micro-102215-095308

2 Blair, J. M. A., Webber, M. A., Baylay, A. J., Ogbolu, D. O. & Piddock, L. J. V. Molecular mechanisms of antibiotic resistance. *Nature Reviews Microbiology* **13**, 42-51 (2015). https://doi.org/10.1038/nrmicro3380

3 Fivenson, E. M. *et al.* A role for the Gram-negative outer membrane in bacterial shape determination. *Proc Natl Acad Sci U S A* **120**, e2301987120 (2023). https://doi.org/10.1073/pnas.2301987120

4 Rojas, E. R. *et al.* The outer membrane is an essential load-bearing element in Gram-negative bacteria. *Nature* **559**, 617-621 (2018). https://doi.org/10.1038/s41586-018-0344-3

5 Deghelt, M. *et al.* Peptidoglycan-outer membrane attachment generates periplasmic pressure to prevent lysis in Gram-negative bacteria. *Nat Microbiol* **10**, 1963-1974 (2025). https://doi.org/10.1038/s41564-025-02058-9

6 Cameron, T. A. & Margolin, W. Insights into the assembly and regulation of the bacterial divisome. *Nat Rev Microbiol* **22**, 33-45 (2024). https://doi.org/10.1038/s41579-023-00942-x

7 Navarro, P. P. *et al.* Cell wall synthesis and remodelling dynamics determine division site architecture and cell shape in *Escherichia coli*. *Nat Microbiol* **7**, 1621-1634 (2022). https://doi.org/10.1038/s41564-022-01210-z

8 Weigand, R. A., Vinci, K. D. & Rothfield, L. I. Morphogenesis of the bacterial division septum: a new class of septation-defective mutants. *Proceedings of the National Academy of Sciences* **73**, 1882-1886 (1976). https://doi.org/doi:10.1073/pnas.73.6.1882

9 Fung, J., MacAlister, T. J. & Rothfield, L. I. Role of murein lipoprotein in morphogenesis of the bacterial division septum: phenotypic similarity of lkyD and lpo mutants. *J Bacteriol* **133**, 1467-1471 (1978). https://doi.org/10.1128/jb.133.3.1467-1471.1978

10 Judd, E. M. *et al.* Distinct constrictive processes, separated in time and space, divide caulobacter inner and outer membranes. *J Bacteriol* **187**, 6874-6882 (2005). https://doi.org/10.1128/JB.187.20.6874-6882.2005

11 Szczepaniak, J. *et al.* The lipoprotein Pal stabilises the bacterial outer membrane during constriction by a mobilisation-and-capture mechanism. *Nature communications* **11**, 1305 (2020). https://doi.org/10.1038/s41467-020-15083-5

12 Gerding, M. A., Ogata, Y., Pecora, N. D., Niki, H. & de Boer, P. A. The trans-envelope Tol-Pal complex is part of the cell division machinery and required for proper outer-membrane invagination during cell constriction in *E. coli*. *Mol Microbiol* **63**, 1008-1025 (2007). https://doi.org/10.1111/j.1365-2958.2006.05571.x

13 Mathelie-Guinlet, M., Asmar, A. T., Collet, J. F. & Dufrene, Y. F. Lipoprotein Lpp regulates the mechanical properties of the *E. coli* cell envelope. *Nature communications* **11**, 1789 (2020). https://doi.org/10.1038/s41467-020-15489-1

14 Sheng, Q. *et al.* In situ visualization of Braun's lipoprotein on *E. coli* sacculi. *Sci Adv* **9**, eadd8659 (2023). https://doi.org/10.1126/sciadv.add8659

15 Mamou, G. *et al.* Peptidoglycan maturation controls outer membrane protein assembly. *Nature* **606**, 953-959 (2022). https://doi.org/10.1038/s41586-022-04834-7

16 Gray, A. N. *et al.* Coordination of peptidoglycan synthesis and outer membrane constriction during *Escherichia coli* cell division. *Elife* **4** (2015). https://doi.org/10.7554/eLife.07118

17 Typas, A. *et al.* Regulation of peptidoglycan synthesis by outer-membrane proteins. *Cell* **143**, 1097-1109 (2010). https://doi.org/10.1016/j.cell.2010.11.038

18 Paradis-Bleau, C. *et al.* Lipoprotein cofactors located in the outer membrane activate bacterial cell wall polymerases. *Cell* **143**, 1110-1120 (2010). https://doi.org/10.1016/j.cell.2010.11.037

19 Reusch, R. N. Insights into the structure and assembly of *Escherichia coli* outer membrane protein A. *FEBS J* **279**, 894-909 (2012). https://doi.org/10.1111/j.1742-4658.2012.08484.x

20 Kroos, L. *et al.* Milestones in the development of *Myxococcus xanthus* as a model multicellular bacterium. *J Bacteriol* **207**, e0007125 (2025). https://doi.org/10.1128/jb.00071-25

21 De Santiago, C. B., Topo, E. J., Cao, P., Wall, D. & Nan, B. A SNARE-like mechanism mediates bacterial outer membrane exchange. *bioRxiv*, 2025.2004.2025.650704 (2025). https://doi.org/10.1101/2025.04.25.650704

22 Remis, J. P. *et al.* Bacterial social networks: structure and composition of *Myxococcus xanthus* outer membrane vesicle chains. *Environ Microbiol* **16**, 598-610 (2014). https://doi.org/10.1111/1462-2920.12187

23 Subedi, K., Roy, P. C., Saiz, B., Basile, F. & Wall, D. Cell-cell transfer of adaptation traits benefits kin and actor in a cooperative microbe. *Proc Natl Acad Sci U S A* **121**, e2402559121 (2024). https://doi.org/10.1073/pnas.2402559121

24 Nan, B. & Zusman, D. R. Uncovering the mystery of gliding motility in the myxobacteria. *Annu Rev Genet* **45**, 21-39 (2011). https://doi.org/10.1146/annurev-genet-110410-132547

25 Nan, B. & Zusman, D. R. Novel mechanisms power bacterial gliding motility. *Mol Microbiol* **101**, 186-193 (2016). https://doi.org/10.1111/mmi.13389

26 Oldewurtel, E. R., Kitahara, Y. & van Teeffelen, S. Robust surface-to-mass coupling and turgor-dependent cell width determine bacterial dry-mass density. *Proc Natl Acad Sci U S A* **118** (2021). https://doi.org/10.1073/pnas.2021416118

27 Pilizota, T. & Shaevitz, J. W. Plasmolysis and cell shape depend on solute outer-membrane permeability during hyperosmotic shock in *E. coli*. *Biophys J* **104**, 2733-2742 (2013). https://doi.org/10.1016/j.bpj.2013.05.011

28 Harvey, C. W., Madukoma, C. S., Mahserejian, S., Alber, M. S. & Shrout, J. D. Cell division resets polarity and motility for the bacterium *Myxococcus xanthus*. *J Bacteriol* **196**, 3853-3861 (2014). https://doi.org/10.1128/JB.02095-14

29 Yang, Z., Lux, R., Hu, W., Hu, C. & Shi, W. PilA localization affects extracellular polysaccharide production and fruiting body formation in *Myxococcus xanthus*. *Mol Microbiol* **76**, 1500-1513 (2010). https://doi.org/10.1111/j.1365-2958.2010.07180.x

30 Zhou, T. & Nan, B. Exopolysaccharides promote *Myxococcus xanthus* social motility by inhibiting cellular reversals. *Mol Microbiol* **103**, 729-743 (2017). https://doi.org/10.1111/mmi.13585

31 Dubois, L., Vettiger, A., Buss, J. A. & Bernhardt, T. G. Using fluorescently labeled wheat germ agglutinin to track lipopolysaccharide transport to the outer membrane in *Escherichia coli*. *mBio* **16**, e0395024 (2025). https://doi.org/10.1128/mbio.03950-24

32 Nan, B. *et al.* Flagella stator homologs function as motors for myxobacterial gliding motility by moving in helical trajectories. *Proc Natl Acad Sci U S A* **110**, E1508-1513 (2013). https://doi.org/10.1073/pnas.1219982110

33 Wei, X., Pathak, D. T. & Wall, D. Heterologous protein transfer within structured myxobacteria biofilms. *Mol Microbiol* **81**, 315-326 (2011). https://doi.org/10.1111/j.1365-2958.2011.07710.x

34 Hsu, Y. P. *et al.* Full color palette of fluorescent d-amino acids for in situ labeling of bacterial cell walls. *Chem Sci* **8**, 6313-6321 (2017). https://doi.org/10.1039/c7sc01800b

35 Fu, G. *et al.* MotAB-like machinery drives the movement of MreB filaments during bacterial gliding motility. *Proc Natl Acad Sci U S A* **115**, 2484-2489 (2018). https://doi.org/10.1073/pnas.1716441115

36 Nan, B. *et al.* The polarity of myxobacterial gliding is regulated by direct interactions between the gliding motors and the Ras homolog MglA. *Proc Natl Acad Sci U S A* **112**, E186-193 (2015). https://doi.org/10.1073/pnas.1421073112

37 Tokunaga, M., Imamoto, N. & Sakata-Sogawa, K. Highly inclined thin illumination enables clear single-molecule imaging in cells. *Nat Methods* **5**, 159-161 (2008). https://doi.org/10.1038/nmeth1171

38 Treuner-Lange, A. *et al.* PomZ, a ParA-like protein, regulates Z-ring formation and cell division in *Myxococcus xanthus*. *Mol Microbiol* **87**, 235-253 (2013). https://doi.org/10.1111/mmi.12094

39 Aramayo, R. & Nan, B. *De Novo* Assembly and Annotation of the Complete Genome Sequence of *Myxococcus xanthus* DZ2. *Microbiol Resour Announc*, e0107421 (2022). https://doi.org/10.1128/mra.01074-21

40 Iniesta, A. A., Garcia-Heras, F., Abellon-Ruiz, J., Gallego-Garcia, A. & Elias-Arnanz, M. Two systems for conditional gene expression in *Myxococcus xanthus* inducible by isopropyl-beta-D-thiogalactopyranoside or vanillate. *J Bacteriol* **194**, 5875-5885 (2012). https://doi.org/10.1128/JB.01110-12

41 Magnet, S. *et al.* Identification of the L,D-transpeptidases responsible for attachment of the Braun lipoprotein to *Escherichia coli* peptidoglycan. *J Bacteriol* **189**, 3927-3931 (2007). https://doi.org/10.1128/JB.00084-07

42 Sun, J., Rutherford, S. T., Silhavy, T. J. & Huang, K. C. Physical properties of the bacterial outer membrane. *Nat Rev Microbiol* **20**, 236-248 (2022). https://doi.org/10.1038/s41579-021-00638-0

43 Asmar, A. T. *et al.* Communication across the bacterial cell envelope depends on the size of the periplasm. *PLoS Biol* **15**, e2004303 (2017). https://doi.org/10.1371/journal.pbio.2004303

44 Hummels, K. R. *et al.* Coordination of bacterial cell wall and outer membrane biosynthesis. *Nature* **615**, 300-304 (2023). https://doi.org/10.1038/s41586-023-05750-0

45 Asmar, A. T. & Collet, J. F. Lpp, the Braun lipoprotein, turns 50-major achievements and remaining issues. *FEMS Microbiol Lett* **365** (2018). https://doi.org/10.1093/femsle/fny199

46 Szczepaniak, J., Press, C. & Kleanthous, C. The multifarious roles of Tol-Pal in Gram-negative bacteria. *FEMS Microbiol Rev* **44**, 490-506 (2020). https://doi.org/10.1093/femsre/fuaa018

47 Campos, J. M. & Zusman, D. R. Regulation of Development in *Myxococcus-xanthus* - Effect of 3' Doublebond 5'-Cyclic Amp, Adp, and Nutrition. *Proceedings of the National Academy of Sciences of the United States of America* **72**, 518-522 (1975). https://doi.org/DOI 10.1073/pnas.72.2.518

48 Vlamakis, H. C., Kirby, J. R. & Zusman, D. R. The Che4 pathway of *Myxococcus xanthus* regulates type IV pilus-mediated motility. *Mol Microbiol* **52**, 1799-1811 (2004).